

Spatially Resolved Studies of Local Massive Red Spiral Galaxies

CAI-NA HAO,¹ YONG SHI,^{2,3} YANMEI CHEN,^{2,3} XIAOYANG XIA,¹ QIUSHENG GU,^{2,3} RUI GUO,¹
 XIAOLING YU,^{2,3} AND SONGLIN LI^{2,3}

¹*Tianjin Astrophysics Center, Tianjin Normal University, Tianjin 300387, China*

²*School of Astronomy and Space Science, Nanjing University, Nanjing 210093, China*

³*Key Laboratory of Modern Astronomy and Astrophysics (Nanjing University), Ministry of Education, Nanjing 210093, China*

Submitted to ApJL

ABSTRACT

We report two-dimensional spectroscopic analysis of massive red spiral galaxies ($M_* > 10^{10.5} M_\odot$) and compare them to blue spiral and red elliptical galaxies above the same mass limit based on the public SDSS DR15 MaNGA observations. We find that the stellar population properties of red spiral galaxies are more similar to those of elliptical galaxies than to blue spiral galaxies. Red spiral galaxies show a shallow mass-weighted age profile, and they have higher stellar metallicity and $Mgb/\langle Fe \rangle$ across the whole $1.5R_e$ as compared to blue spirals, but all these properties are close to those of elliptical galaxies. One scenario to explain this is that red spirals form as remnants of very gas-rich major mergers that happened above $z \sim 1$.

Keywords: galaxies: evolution galaxies: formation

1. INTRODUCTION

The global properties of galaxies show bimodality in both optical colors and morphologies, and these two properties are closely linked to each other: spiral galaxies are mostly blue and elliptical galaxies appear red (Baldry et al. 2004; Bell et al. 2004; Schawinski et al. 2014). It is generally believed that a spiral galaxy grows its disk inside-out through a gradual mode by long-standing gas accretion and moderate star formation rates (Mo et al. 1998; Munoz-Mateos et al. 2007), and a massive elliptical galaxy is produced through an intense mode in which merging of two spiral galaxies triggers strong starbursts and transforms morphologies violently (Hopkins et al. 2006). However, the existence of red passive spiral galaxies, those with spiral morphologies but red colors (little star formation), poses a challenge to the above popular scenarios (Bundy et al. 2010; Masters et al. 2010). They could be a special phase during secular evolution in which star formation has already ceased but morphologies stay intact due to the lack of violent events, such as major mergers (Masters et al. 2010). They could also be products of some other physical processes, e.g., galaxy merging with high

gas fractions that instead produces spiral galaxies (Springel & Hernquist 2005; Robertson et al. 2006; Robertson & Bullock 2008; Hopkins et al. 2009; Athanassoula et al. 2016; Sparre & Springel 2017).

Many efforts have been devoted to understanding the origin of red spiral galaxies (e.g., Skibba et al. 2009; Robaina et al. 2012). Existing investigations of red spirals revealed some distinct properties as compared to normal blue spirals (Bundy et al. 2010; Masters et al. 2010; Tojeiro et al. 2013): their star formation rates and dust contents are low with old central stellar populations as expected from their red colors; they reside in all kinds of environments with preference in intermediate local densities; they have higher fractions of Seyferts and LINERs (Low Ionization Nuclear Emission Regions) and significantly higher bar fractions; their stellar light distributions are more concentrated. However, investigations of spectroscopic properties of their stellar populations are limited.

In Guo et al. (2019, submitted, hereafter Paper I), we selected a red massive spiral galaxy sample from the Sloan Digital Sky Survey Data Release 7 (SDSS DR7) and compared their central and global properties with those of blue spiral and red elliptical galaxies based on the SDSS fiber spectra and photometric data. We found that red spirals are more similar to red ellipticals than to blue spirals of comparable masses in their central stellar populations, stellar mass surface densities and host dark matter halo masses. These results suggest that the central parts of red spiral galaxies formed at a similar epoch and timescale to those of red ellipticals. Our Paper I and previous studies from other groups (Masters et al. 2010; Robaina et al. 2012; Tojeiro et al. 2013) are mainly based on the fiber spectra from SDSS, which can only sample the bulge component of local red spiral galaxies. It is essential to extend similar studies to disk components to have a more complete census of their stellar populations.

In this paper, we explore the two-dimensional spectroscopic data as observed by the survey of the Mapping Nearby Galaxies at Apache Point Observatory (MaNGA) (Bundy et al. 2015; Drory et al. 2015; Law et al. 2015, 2016; Yan et al. 2016a,b; Blanton et al. 2017; Wake et al. 2017). Such data enable constraints on the spatial distributions of kinematics and stellar population properties such as age, metallicity and α -element enhancement, which will provide important clues to the origin of red spiral galaxies. We adopt a flat Λ CDM cosmology with $\Omega_m = 0.3$, $\Omega_\Lambda = 0.7$, $H_0 = 70 \text{ km s}^{-1} \text{ Mpc}^{-1}$.

2. SAMPLE SELECTION AND MANGA DATA

Our sample of massive red spiral galaxies with stellar masses above $10^{10.5} M_\odot$ is selected from the SDSS DR7 (Abazajian et al. 2009), with their dust-corrected $u - r$ color in the red sequence (see Figure 1 (a)) and spiral features in their morphologies (see Figure 1 (b)). To better understand their origin, we compare red spirals to blue spirals and red ellipticals above the same mass limit, as shown in Figure 1 (a). The sample selection is detailed in Paper I. Briefly, galaxies with redshift of $0.02 < z < 0.05$ and stellar masses above $10^{10.5} M_\odot$ were selected from the catalog of Mendel et al. (2014). The morphological information from the Galaxy Zoo 1 project (Lintott et al. 2011) was then adopted to divide the sample into spirals and ellipticals. To minimize the impact of the dust attenuation, spirals with disc inclination angle $i > 60 \text{ deg}$ were rejected. Then spirals and ellipticals were separated into blue and red according to their locations in the dust-corrected $u - r$ color versus stellar mass diagram following similar criteria in Guo et al. (2016) (see Figure 1 (a)). After cross-matching these galaxies with the data release 15 of the SDSS for the MaNGA (Bundy et al. 2015; Law et al. 2015; Aguado et al. 2019), we were left with 22 red spirals, along with 50 blue spirals and 164 red ellipticals, plotted in Figure 1 (a). As can be seen from this figure, red spirals and ellipticals span a wider range in mass than blue spirals towards the high mass end. Considering possible effects

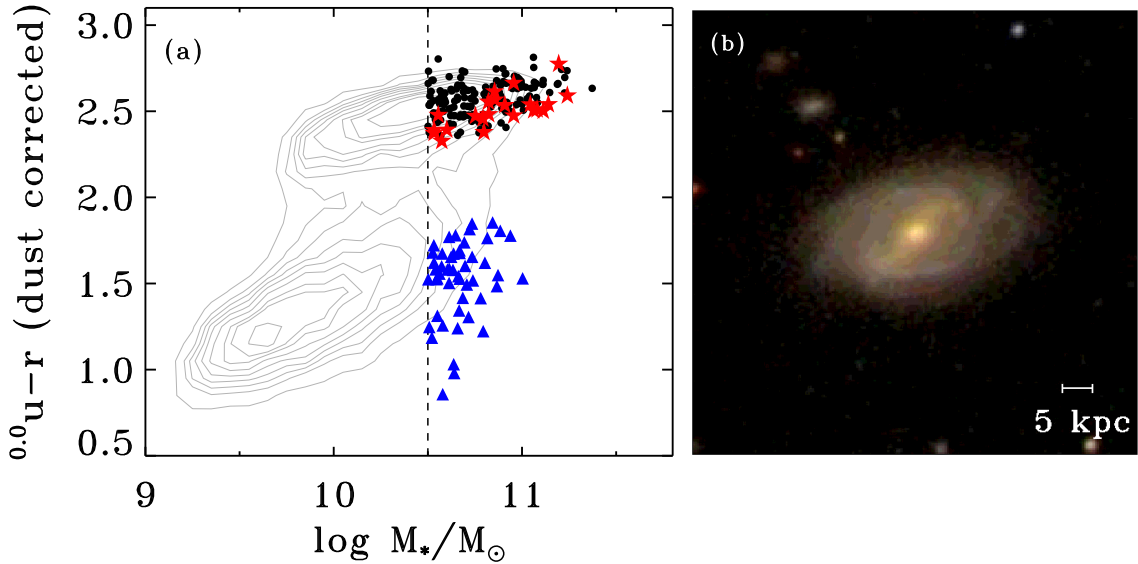


Figure 1. Selections of samples. (a), massive red spiral galaxies (red symbols) are selected using the $u-r$ color vs. stellar mass diagram from the SDSS, along with blue spirals (blue symbols) and red ellipticals (black symbols). The contours show the number density distribution of galaxies in the redshift range of $0.02 < z < 0.05$ and absolute z -band magnitude of $M_{z,\text{Petro}} < -19.5$ in the catalog of Mendel et al. (2014). The dashed line marked the stellar mass of $10^{10.5} M_{\odot}$. (b), an SDSS false-color image of a red spiral galaxy.

of the mass dependence of the stellar population and kinematic properties, we extracted subsamples by restricting the stellar masses to the range of $10^{10.5} - 10^{11} M_{\odot}$, which yields 15 red spirals, 49 blue spirals and 139 ellipticals. We will study both the samples with $M_{*} > 10^{10.5} M_{\odot}$ (referred to “the main samples”, hereafter) to keep the sample sizes as large as possible and the subsamples with $10^{10.5} < M_{*} < 10^{11} M_{\odot}$ to minimize the mass dependence effect. Since only one blue spiral galaxy was removed from the main sample to form the subsample, we do not expect any changes in their properties. We note that our samples of galaxies are not complete samples but they should be representative of the respective types of galaxies.

The MaNGA data analysis pipeline (Westfall et al. 2019), which uses pPXF (Cappellari et al. 2004; Cappellari 2017) and the MIUSCAT (Vazdekis et al. 2012) stellar library, fits the stellar continuum in each spaxel and produces estimates of the stellar kinematics and lick indices, including V_{star} , σ_{star} and $\text{Mgb}/\langle\text{Fe}\rangle$ ($=\text{Mgb}/(0.5*\text{Fe}5270+0.5*\text{Fe}5335)$) used in this study. The stellar metallicity and stellar age are taken from the MaNGA Pipe3D value added catalog (Sánchez et al. 2016, 2018) included in the SDSS DR 15. To investigate the formation of the bulk of the stars in galaxies, we use the stellar mass-weighted ages and metallicities in this work. Median radial profiles of the above quantities will be used to characterize the properties of each type of galaxies. They are the azimuthally averaged radial profiles of galaxies within each category. To better understand the properties of the bulge and disk components for spiral galaxies, we adopt the effective radius of the bulge component as a measure of the bulge size, which was derived by Sersic+Exponential fitting to the 2D surface brightness profile of the SDSS r -band image (Fischer et al. 2019). The median bulge sizes for red

and blue spirals are around¹ $0.15 R_e$ and $0.3 R_e$, respectively, where R_e is the effective radius of the total light distribution.

3. RESULTS

We first examine the kinematics of our three types of galaxies to verify whether the kinematic estimator of morphologies are consistent with the optical one. Figure 2 (a) shows the median radial profile of the ratio of rotation velocity to velocity dispersion for blue spiral, red spiral and elliptical galaxies in the main samples. The red and blue arrows indicate the median bulge size of red spiral and blue spiral galaxies, respectively. As shown in the figure, red spiral galaxies have similar kinematics to blue spirals, with dispersion-dominated bulges in the inner regions plus the rotation-dominated disks in the outer regions. Elliptical galaxies show dispersion-dominated kinematics from the central part to the outer part. Figure 2 (a) confirms the optical morphological classification that red spirals do harbor bulges and rotating disks. The results for the subsamples are shown in Figure 2 (b). For both ellipticals and blue spirals, the $V_{\text{star}}/\sigma_{\text{star}}$ profiles stay the same as those for the main samples. By contrast, red spirals show remarkably lower ratios of velocity to velocity dispersion in their disks than the main sample, which is mainly caused by the decrease in the rotational velocity as we examined, a result of the Tully-Fisher relation (Tully & Fisher 1977). But they are still consistent with being systems harboring bulges and rotating disks.

In Figure 3, we present the median radial profiles of the stellar population properties of the three types of galaxies including stellar ages, metallicities and $\text{Mgb}/\langle\text{Fe}\rangle$. Figure 3 (a)-(c) are for the main samples of galaxies. As shown in Figure 3 (a), red spirals and elliptical galaxies show similar shallow age profiles out to $1.5 R_e$, although red spirals are slightly younger than ellipticals. As labeled in the y-axis of the figure, red spirals formed their bulge and disk components within ~ 1.5 Gyr before redshift $\sim 1.2 - 1.3$, and ellipticals formed within ~ 1 Gyr before redshift ~ 1.5 . In contrast, the central region ($< 0.3 R_e$) of blue spirals shows a steep mass-weighted age gradient with similar ages to red spirals and ellipticals at the very center, while their disk components show flat age gradients but are much younger than red spirals and ellipticals. The above results suggest that red spirals most likely harbor star formation histories that resemble ellipticals instead of blue spirals. Blue spirals started to form their bulges at a similar time to red spirals but have an extended star formation history in the outer parts, which is consistent with a prolonged inside-out formation scenario.

Figure 3 (b) presents the median radial profiles of the stellar metallicities. Red spirals show a rather flat metallicity profile from the center out to $1.5 R_e$. Blue spiral galaxies and ellipticals show similarly steeper metallicity gradients than red spirals, with blue spirals being more metal-poor than ellipticals. Compared to red spirals, blue spirals are more metal-poor over the entire probed radius, and the metallicity difference varies from ~ 0.03 dex to ~ 0.1 dex. On the other hand, elliptical galaxies are more metal-rich in the inner region ($\lesssim 0.5 - 0.6 R_e$) but more metal-poor in the outer region ($\gtrsim 0.5 - 0.6 R_e$) than red spirals.

Figure 3 (c) shows the median radial profiles of $\text{Mgb}/\langle\text{Fe}\rangle$. Mgb is used to probe the α elements (e.g., Worthey et al. 1992; Zheng et al. 2019) that are produced by type II supernova, while Fe is synthesized in type Ia supernova. The α/Fe ratio traces the relative importance of the intense starburst and the subsequent long-term quiescent star formation (Matteucci & Greggio 1986; Worthey et al. 1992; Thomas et al. 2005). As shown in the figure, the $\text{Mgb}/\langle\text{Fe}\rangle$ profile of red spirals breaks into

¹ The main samples and the subsamples show slightly different median bulge sizes.

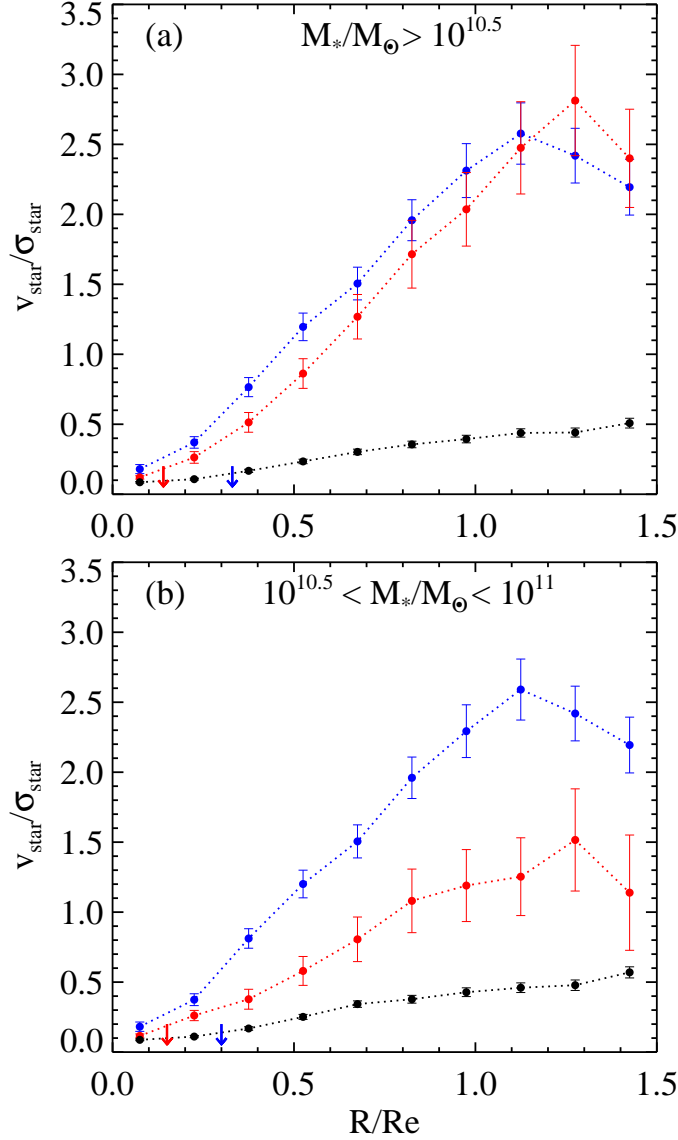


Figure 2. The median radial profiles of $V_{\text{star}}/\sigma_{\text{star}}$ for red spiral galaxies (red), blue spiral galaxies (blue) and red elliptical galaxies (black) in the main samples (a) and in the subsamples (b), with a radial bin of $0.15 R_e$. The error bar represents the error of the mean. The downward arrows indicate the median effective radius of the bulge component for red spirals (red) and blue spirals (blue).

three parts: flat profiles in the inner ($\lesssim 0.5R_e$) and outer regions ($\gtrsim 0.8R_e$), and an intermediate declining profile connecting the higher $\log(\text{Mgb}/\langle\text{Fe}\rangle)$ values (~ 0.23) in the inner region and the lower $\log(\text{Mgb}/\langle\text{Fe}\rangle)$ values (~ 0.16) in the outer region. In comparison, elliptical galaxies show a very flat $\text{Mgb}/\langle\text{Fe}\rangle$ profile and high $\log(\text{Mgb}/\langle\text{Fe}\rangle)$ values about 0.22. Blue spirals also have a flat

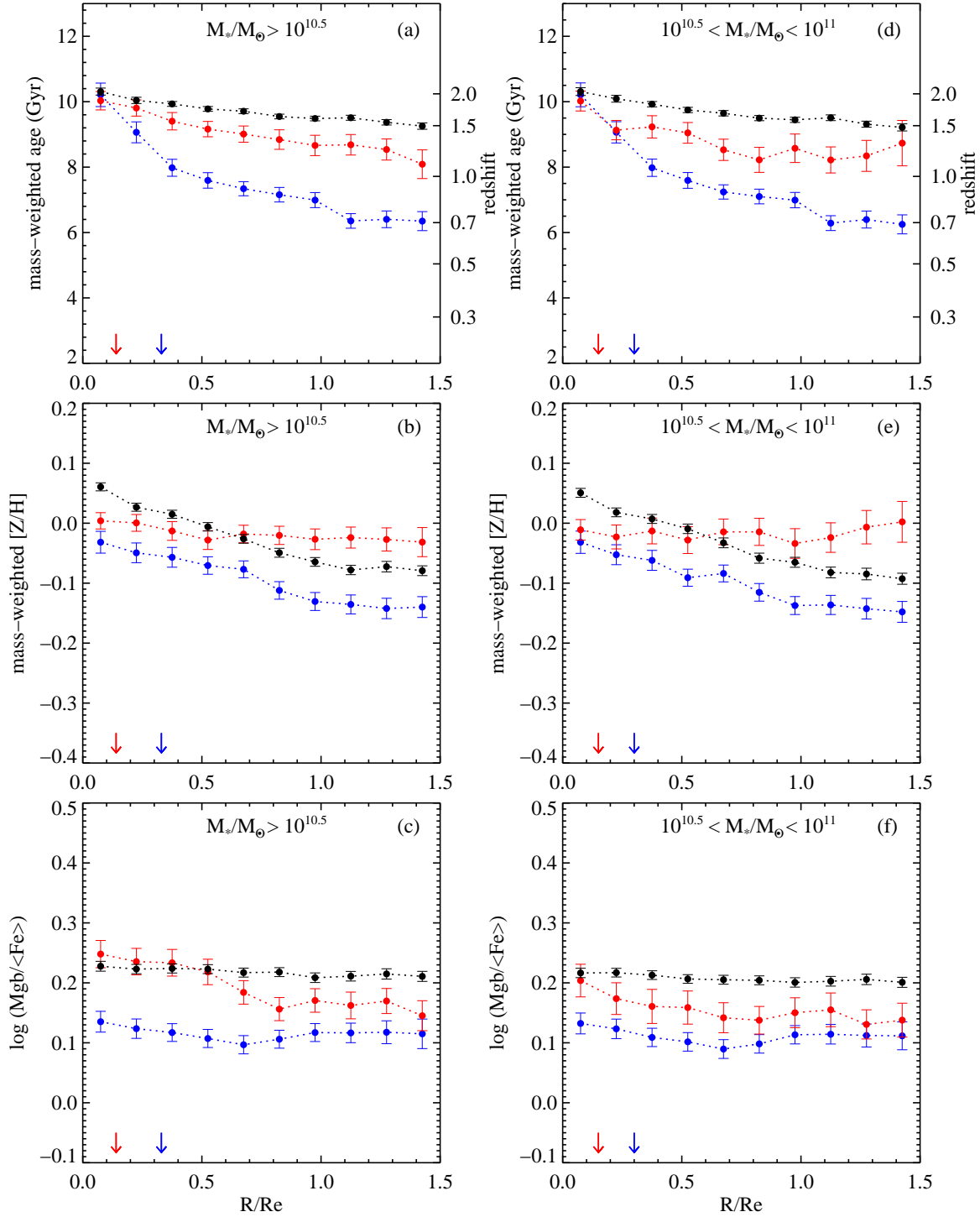


Figure 3. The median radial profiles of stellar mass-weighted age (a), stellar mass-weighted metallicity (b), and $\log(Mgb/\langle Fe \rangle)$ (c) for red spiral galaxies (red), blue spiral galaxies (blue) and red elliptical galaxies (black) in the main samples. The same properties for the subsamples are shown in (d)-(f). The data points connected by dotted lines show the profiles along the ellipse with position angle and ellipticity from NASA-Sloan Atlas (Abazajian et al. 2009; Blanton et al. 2011). The bin sizes are 0.15 R_e . The error bar represents the error of the mean. The downward arrows indicate the median effective radius of the bulge component for red spirals (red) and blue spirals (blue).

Mgb/ $\langle\text{Fe}\rangle$ profile but their $\log(\text{Mgb}/\langle\text{Fe}\rangle)$ values are relatively low (~ 0.12). The higher values of Mgb/ $\langle\text{Fe}\rangle$ for elliptical galaxies suggest a short star formation timescale while the lower values of Mgb/ $\langle\text{Fe}\rangle$ for blue spiral galaxies reflect the contribution of a more prolonged star formation history. The Mgb/ $\langle\text{Fe}\rangle$ values in the bulge and the inner region of the disk of red spiral galaxies are comparable to those of elliptical galaxies, implying similarly short star formation timescales in the inner region of red spiral galaxies and elliptical galaxies. On the other hand, the intermediate Mgb/ $\langle\text{Fe}\rangle$ values in the disk components of red spiral galaxies suggest a star formation timescale between those of ellipticals and blue spirals.

Similar to Figure 3 (a)-(c), Figure 3 (d)-(f) show the median radial profiles of stellar ages, metallicities and Mgb/ $\langle\text{Fe}\rangle$ but for the subsamples of galaxies with stellar masses $10^{10.5} < M_* < 10^{11} M_\odot$. It is obvious that this further stellar mass cut at the high mass end does not change the results for ellipticals and blue spirals. Even for red spirals, both the profiles of the stellar ages and metallicities are similar to the main samples. The only notable change is in the Mgb/ $\langle\text{Fe}\rangle$ profile of red spirals at $R \lesssim 0.7R_e$. Red spirals in the subsample show lower Mgb/ $\langle\text{Fe}\rangle$ values than those in the main sample, which suggests that more massive red spirals have higher Mgb/ $\langle\text{Fe}\rangle$ and hence shorter star formation timescales in their inner regions. In spite of this decrease in the Mgb/ $\langle\text{Fe}\rangle$ values, they are still larger than blue spirals. This suggests that the star formation timescales of red spirals are in between the ellipticals and blue spirals except the most central (bulge) region that shows an identical Mgb/ $\langle\text{Fe}\rangle$ value with the ellipticals. In summary, the subsample of red spirals shows some different properties from the main sample in their disk components, but this does not affect the relative difference between these three types of galaxies.

4. DISCUSSION

The stellar population properties presented in Figure 3 for blue spiral galaxies and elliptical galaxies are in good agreement with those shown in the literature (e.g., González Delgado et al. 2015; Zheng et al. 2017). Blue spiral galaxies have an extended star formation history with their bulge components formed earlier than their disk components, consistent with the inside-out formation scenario as induced by long-standing gas accretion and associated star formation. Elliptical galaxies show old stellar ages and enhanced Mgb/ $\langle\text{Fe}\rangle$ values, in agreement with the early formation epoch and short star formation timescales.

While studies of morphologies and kinematics of red spirals indicate that they harbor typical spiral disks in addition to the central bulges, their stellar populations are instead found to be distinctly different from blue spirals: red spirals have an older and shallower mass-weighted age profile than blue spirals, with their disks younger than their bulges by $\sim 1 - 2$ Gyr; they show a more metal-rich and flatter mass-weighted metallicity profile relative to blue spirals; their Mgb/ $\langle\text{Fe}\rangle$ values are in between ellipticals and blue spirals, being enhanced compared to blue spirals.

The above results suggest that red spiral galaxies are not evolutionary remnants of blue spiral galaxies. Instead, they are consistent with the remnant of galaxy merging with high gas fractions. While in general galaxy merging produces elliptical galaxies (Hopkins et al. 2006), theoretical simulations predicted that merging with high gas fractions ($f_{\text{gas}} > 0.5$ at the time of merger; e.g., Robertson et al. 2006) instead produces spiral galaxies (Springel & Hernquist 2005; Robertson et al. 2006; Hopkins et al. 2009; Athanassoula et al. 2016; Sparre & Springel 2017). During such a very gas-rich major merger, gravitational torques make gas within some characteristic radius lose angular momentum and fall into the center rapidly, and then form stars in a starburst mode (Hopkins et al. 2009).

This process leads to the formation of a bulge component with high metallicity and $\text{Mgb}/\langle\text{Fe}\rangle$. On the other hand, gas at sufficiently large radii that cannot fall in efficiently, or gas that cannot efficiently dissipate or lose the angular momentum will cool quickly and re-form a rotating disk. Subsequently, the gas in the disk form stars but with much reduced star formation rates (Springel & Hernquist 2005), which will result in a new stellar disk with younger age and lower $\text{Mgb}/\langle\text{Fe}\rangle$ than the bulge formed earlier in the starburst. The disk can still have similar metallicity to the bulge assuming the galaxy is quenched soon after formation. All these theoretical expectations are in good agreement with our observational results shown in Figure 3.

Furthermore, we note that very gas-rich major merging events may only happen at relatively high redshifts (above $z \sim 1$) when the gas content was rich. This condition could be satisfied, as shown by the old stellar populations of red spirals in Figure 3(a). If the proposed scenario is plausible, red spirals thus offer a window to understanding the formation of massive spiral galaxies through gas-rich major mergers instead of the gradual inside-out growth mode.

The most difficult part of the merging scenario is to explain the shutdown of the star formation in red spirals. The IFU data shown here could not put any constraints on the star formation quenching mechanisms. But the investigations on the bulge to total stellar mass ratios and the halo masses in our paper I provide some hints on possible quenching mechanisms. Red spiral galaxies show higher bulge to total stellar mass ratios than blue spiral galaxies and more than 80% of red spiral galaxies are hosted by dark matter halos heavier than $10^{12}M_{\odot}$, above which halo quenching takes effect. So morphological quenching (Martig et al. 2009) may be responsible for the cease of the star formation and the massive dark matter halos may have been preventing gas from cooling and falling onto the galaxies to form new stars.

5. CONCLUSION

We carried out two-dimensional spectroscopic analysis of massive red spiral galaxies with $M_{*} > 10^{10.5} M_{\odot}$ out to $1.5R_e$, and compared them to blue spiral and red elliptical galaxies above the same mass limit based on the SDSS DR 15 for the MaNGA survey. We found that the stellar population properties of red spiral galaxies are more similar to those of red elliptical galaxies than to blue spiral galaxies. They have higher stellar metallicity and $\text{Mgb}/\langle\text{Fe}\rangle$ across the whole $1.5R_e$ as compared to blue spirals, and their stars are old with relatively flat mass-weighted age gradients in contrast to those of blue spiral galaxies. These results prove that red spiral galaxies are not evolutionary remnants of blue spiral galaxies. They are possible remnants of gas-rich major mergers above $z \sim 1$ instead. Major mergers of disk galaxies with sufficiently high gas content can form a bulge rapidly in the first place and then form a gas disk. The gas in the disk will form stars subsequently.

We thank the anonymous referee for constructive comments that improved the paper. We would like to thank Drs. Cheng Li, Shude Mao, Dandan Xu, Zheng Zheng, Fangzhou Jiang, and Jian Fu for helpful discussions. This work is supported by the National Key Research and Development Program of China (No. 2017YFA0402703) and the National Natural Science Foundation of China (NSFC, No. 11733002 and 11373027). Y.S. also acknowledges the support from the National Key R&D Program of China (No. 2018YFA0404502, No. 2017YFA0402704), the NSFC (No. 11825302, 11773013) and the Excellent Youth Foundation of the Jiangsu Scientific Committee (BK20150014). Y.C. also acknowledges the support from the National Key R&D Program of China (No. 2017YFA0402704) and the NSFC (No. 11573013). Funding for the Sloan Digital Sky Survey IV has been provided by the

Alfred P. Sloan Foundation, the U.S. Department of Energy Office of Science, and the Participating Institutions. SDSS-IV acknowledges support and resources from the Center for High-Performance Computing at the University of Utah. The SDSS web site is www.sdss.org. SDSS-IV is managed by the Astrophysical Research Consortium for the Participating Institutions of the SDSS Collaboration including the Brazilian Participation Group, the Carnegie Institution for Science, Carnegie Mellon University, the Chilean Participation Group, the French Participation Group, Harvard-Smithsonian Center for Astrophysics, Instituto de Astrofísica de Canarias, The Johns Hopkins University, Kavli Institute for the Physics and Mathematics of the Universe (IPMU) / University of Tokyo, the Korean Participation Group, Lawrence Berkeley National Laboratory, Leibniz Institut für Astrophysik Potsdam (AIP), Max-Planck-Institut für Astronomie (MPIA Heidelberg), Max-Planck-Institut für Astrophysik (MPA Garching), Max-Planck-Institut für Extraterrestrische Physik (MPE), National Astronomical Observatories of China, New Mexico State University, New York University, University of Notre Dame, Observatório Nacional / MCTI, The Ohio State University, Pennsylvania State University, Shanghai Astronomical Observatory, United Kingdom Participation Group, Universidad Nacional Autónoma de México, University of Arizona, University of Colorado Boulder, University of Oxford, University of Portsmouth, University of Utah, University of Virginia, University of Washington, University of Wisconsin, Vanderbilt University, and Yale University. This project makes use of the MaNGA-Pipe3D data products. We thank the IA-UNAM MaNGA team for creating this catalogue, and the ConaCyt-180125 project for supporting them.

REFERENCES

- Abazajian, K. N., Adelman-McCarthy, J. K., Agüeros, M. A., et al. 2009, *ApJS*, 182, 543
- Aguado, D. S., Ahumada, R., Almeida, A., et al. 2019, *ApJS*, 240, 23
- Athanassoula, E., Rodionov, S. A., Peschken, N., & Lambert, J. C. 2016, *ApJ*, 821, 90
- Baldry, I. K., Glazebrook, K., Brinkmann, J., et al. 2004, *ApJ*, 600, 681
- Bell, E. F., Wolf, C., Meisenheimer, K., et al. 2004, *ApJ*, 608, 752
- Blanton, M. R., Bershady, M. A., Abolfathi, B., et al. 2017, *AJ*, 154, 28
- Blanton, M. R., Kazin, E., Muna, D., Weaver, B. A., & Price-Whelan, A. 2011, *AJ*, 142, 31
- Bundy, K., Scarlata, C., Carollo, C. M., et al. 2010, *ApJ*, 719, 1969
- Bundy, K., Bershady, M. A., Law, D. R., et al. 2015, *ApJ*, 798, 7
- Cappellari, M. 2017, *MNRAS*, 466, 798
- Cappellari, M., & Emsellem, E. 2004, *PASP*, 116, 138
- Drory, N., MacDonald, N., Bershady, M. A., et al. 2015, *AJ*, 149, 77
- Fischer, J.-L., Domínguez Sánchez, H., & Bernardi, M. 2019, *MNRAS*, 483, 2057
- González Delgado, R. M., García-Benito, R., Pérez, E., et al. 2015, *A&A*, 581, 103
- Guo, R., Hao, C.-N., Xia, X. Y., Mao, S., & Shi, Y. 2016a, *ApJ*, 826, 30
- Hopkins, P. F., Hernquist, L., Cox, T. J., et al. 2006, *ApJS*, 163, 1
- Hopkins, P. F., Cox, T. J., Younger, J. D., & Hernquist, L. 2009, *ApJ*, 691, 1168
- Law, D. R., Cherinka, B., Yan, R., et al. 2016, *AJ*, 152, 83
- Law, D. R., Yan, R., Bershady, M. A., et al. 2015, *AJ*, 150, 19
- Lintott, C., Schawinski, K., Bamford, S., et al. 2011, *MNRAS*, 410, 166
- Martig, M., Bournaud, F., Teyssier, R., et al. 2009, *ApJ*, 707, 250
- Masters, K. L., Mosleh, M., Romer, A. K., et al. 2010, *MNRAS*, 405, 783
- Matteucci, F., & Greggio, L. 1986, *A&A*, 154, 279
- Mendel, J. T., Simard, L., Palmer, M., Ellison, S. L., & Patton, D. R. 2014, *ApJS*, 210, 3
- Mo, H. J., Mao, S., & White, S. D. M. 1998, *MNRAS*, 295, 319
- Muñoz-Mateos, J. C., Gil de Paz, A., Boissier, S., et al. 2007, *ApJ*, 658, 1006

- Robaina, A. R., Hoyle, B., Gallazzi, A., et al. 2012, *MNRAS*, 427, 3006
- Robertson, B. E., & Bullock, J. S. 2008, *ApJ*, 685, L27
- Robertson, B., Bullock, J. S., Cox, T. J., et al. 2006, *ApJ*, 645, 986
- Sánchez, S. F., Avila-Reese, V., Hernandez-Toledo, H., et al. 2018, *RMxAA*, 54, 217
- Sánchez, S. F., Pérez, E., Sánchez-Blázquez, P., et al. 2016, *RMxAA*, 52, 171
- Schawinski, K., Urry, C. M., Simmons, B. D., et al. 2014, *MNRAS*, 440, 889
- Skibba, R. A., Bamford, S. P., Nichol, R. C., et al. 2009, *MNRAS*, 399, 966
- Sparre, M., & Springel, V. 2017, *MNRAS*, 470, 3946
- Springel, V., & Hernquist, L. 2005, *ApJL*, 622, L9
- Thomas, D., Maraston, C., Bender, R., & Mendes de Oliveira, C. 2005, *ApJ*, 621, 673
- Tojeiro, R., Masters, K. L., Richards, J., et al. 2013, *MNRAS*, 432, 359
- Tully, R. B., & Fisher, J. R. 1977, *A&A*, 54, 661
- Vazdekis, A., Ricciardelli, E., Cenarro, A. J., et al. 2012, *MNRAS*, 424, 157
- Wake, D. A., Bundy, K., Diamond-Stanic, A. M., et al. 2017, *AJ*, 154, 86
- Westfall, K. B., Cappellari, M., Bershadsky, M. A., et al. 2019, arXiv e-prints, arXiv:1901.00856
- Worthey, G., Faber, S. M., & Gonzalez, J. J. 1992, *ApJ*, 398, 69
- Yan, R., Bundy, K., Law, D. R., et al. 2016, *AJ*, 152, 197
- Yan, R., Tremonti, C., Bershadsky, M. A., et al. 2016, *AJ*, 151, 8
- Zheng, Z., Wang, H., Ge, J., et al. 2017, *MNRAS*, 465, 4572
- Zheng, Z., Li, C., Mao, S., et al. 2019, *ApJ*, 873, 63